

Microwave remote sensing of Jupiter's atmosphere from an orbiting spacecraft

M.A. Janssen^{a,*}, M.D. Hofstadter^a, S. Gulkis^a, A.P. Ingersoll^b, M. Allison^c, S.J. Bolton^a,
S.M. Levin^a, L.W. Kamp^a

^a Jet Propulsion Laboratory/Caltech, 4800 Oak Grove Drive, Pasadena, CA 91109, USA

^b 150-21, California Institute of Technology, 1200 E. California Blvd., Pasadena, CA 91125, USA

^c NASA Goddard Institute for Space Studies, 2880 Broadway, New York, NY 10025, USA

Received 17 December 2003; revised 6 August 2004

Available online 13 October 2004

Abstract

Microwave remote sounding from a spacecraft flying by or in orbit around Jupiter offers new possibilities for retrieving important and presently poorly understood properties of its atmosphere. In particular, we show that precise measurements of relative brightness temperature as a function of off-nadir emission angles, combined with absolute brightness temperature measurements, can allow us to determine the global abundances of water and ammonia and study the dynamics and deep circulations of the atmosphere in the altitude range from the ammonia cloud region to depths greater than 30 bars in a manner which would not be achievable with ground-based telescopes.

© 2004 Elsevier Inc. All rights reserved.

Keywords: Jupiter, atmosphere; Abundances, interior; Radio observations; Radiative transfer

1. Introduction

Ground-based work to date, based mainly on high-resolution radio-wavelength observations made at the Very Large Array, has established a thermal spectrum for the integrated disk emission of Jupiter that shows the expected long-wavelength thermal signature of the deep atmosphere (e.g., Berge and Gulkis, 1976; de Pater et al., 2001; Gibson et al., 2004). However, as shown by de Pater et al. (2004), the integrated disk brightness temperature spectrum is difficult to interpret in terms of its deep composition, even if the measurement uncertainties were as low as one might optimistically expect to achieve with a large ground-based radio telescope (2–5%). Causes of this difficulty include accounting for the non-thermal synchrotron radiation that dominates the planet's emission at long wavelengths, uncertainties in atmospheric structure, cloud properties, and the absorption

coefficients of water and ammonia under the conditions of high temperature and pressure encountered in the deep atmosphere.

2. Observation from an orbiting platform

Observation of Jupiter's long-wavelength atmospheric emission from an orbiting spacecraft offers many advantages over Earth-based observations. A spacecraft can fly inside the radiation belts, effectively avoiding the synchrotron emission that obscures the atmospheric thermal emission at longer wavelengths. An orbiting spacecraft allows observations with global coverage and high spatial resolution, made difficult from the VLA because of Jupiter's rotation and the need to perform rotational synthesis to image the planet. For example, Fig. 1 shows the nadir-viewing footprints afforded by an elliptical polar orbit with a perijove of 4500 km at the equator and a $20R_J$ apojove (~ 11 -day period). This figure demonstrates that major dynamical features such as the belts,

* Corresponding author. Fax: +1-818-354-8895.

E-mail address: michael.a.janssen@jpl.nasa.gov (M.A. Janssen).

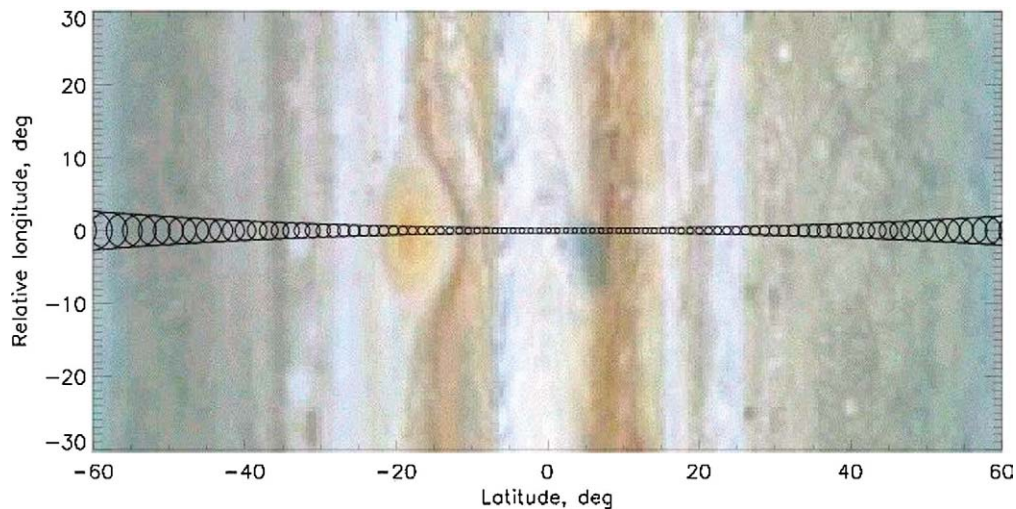


Fig. 1. Nadir footprints for a 10° beam from a nominal elliptical polar orbit (4500 km altitude at perijove, 11-day orbit). A spinning spacecraft is envisioned that scans each radiometer beam along the nadir track, so that each point is observed at a number of emission angles. The density of footprints is much greater than shown.

zones, red spot, and large ovals are readily resolved with the relatively large antenna beams practical at low frequencies from a spacecraft.

An immediate advantage over disk-averaged measurements is given by the ability to observe discrete points in the atmosphere along single lines of sight. The weighting functions and consequent spectral features are more sharply defined for this case than that for a disk average; e.g., by about 10% by our estimation. More importantly, by allowing the spacecraft to rotate so that the beams scan along the nadir track, each point can be viewed at many different emission angles. Absolute calibration at the 2% level or better is achievable in space-borne radiometers (e.g., Ruf et al., 1995; Keihm et al., 2000), comparable to or somewhat better than the ground-based approach. However, the relative brightness temperature, from point to point, or at different emission angles at the same point, can be measured with much higher precision. The ability to collect precise data on the emission angle and spatial dependence of the brightness temperature in combination with the spectrum determination offers an entirely new approach to the microwave sounding of Jupiter.

We estimate that a measurement precision of 0.1% is feasible for relative measurements taken with the same antenna and electronics at the same frequency over short time scales, after accounting for radiometer stability, beam uncertainties, residual synchrotron emission, and imperfect footprint overlap. Intrinsic radiometer noise is easily kept below 0.1% with 1-second signal averaging and modest (10 MHz) receiver bandwidths. Experience with the Cassini microwave radiometer has demonstrated that gain drifts can be maintained at better than this level for minutes to hours in a space environment with current technology (Janssen et al., 2001); further, state-of-the-art microwave noise sources used for gain calibration have demonstrated stability to this level over longer time scales (Tanner, 1998; Tanner and Riley, 2003).

We have investigated the effects of antenna pattern uncertainties and unaccounted emission entering through the sidelobes, including synchrotron emission from Jupiter's radiation belts, to see how these might compromise relative brightness temperature measurements. Within 10,000 km of Jupiter, state-of-the-art antenna design and beam pattern measurement allow the use of beams with $\sim 10^\circ$ half-power widths to obtain relative brightnesses at the 0.1% level, to emission angles as large as 60° , and to at least 40° at much larger distances. Specifically we calculated that the antenna pattern must be known or controlled as follows: (1) main beamwidth to 2%, (2) sidelobes to 30° off-axis measured or suppressed to 30 dB below the central peak, and (3) sidelobes to 40° measured or suppressed to 40 dB. We revised a synchrotron emission model by Levin et al. (2001) to calculate synchrotron emission from the perspective of an orbiting spacecraft and determined that antenna backlobes must be kept below 55 dB at frequencies below 1 GHz to reduce the residual synchrotron contribution to the 0.1% level. Such requirements are within expected capabilities for horn antennas, patch-array and waveguide slot antennas (Rahmat-Samii, private communication, 2004).

Finally, the effect of horizontal variations in the atmosphere is minimized by observing the same locations at different emission angles. The nadir-viewing data can be averaged along-track to equalize the width of the footprint in latitude at off-nadir angles. The distance to the source increases at off-nadir angles, however, and the increased perspective of the longitudinal dimension (e.g., a factor of $\sqrt{3}$ at 60° emission angle) cannot be easily compensated for. On the other hand, the local horizontal variability is readily estimated from the nadir measurements and the consequent limb darkening uncertainty can be well bounded. Janssen et al. (1995) give a technique for estimating errors due to unequal beam footprints when the statistical properties of the measured quantity are known.

3. Modeling Jupiter's atmospheric emission

Our radiative transfer program for computing Jupiter's atmospheric emission is based on the one described in Hofstadter, 1992; and in Hofstadter and Butler, 2003. It assumes a convective atmosphere with constant relative humidity (an adjustable parameter) for each condensable species above its cloud base. Microwave opacity sources include H₂O, NH₃, H₂, and a liquid water cloud, while the model atmosphere also contains He and CH₄. Scattering is neglected. The temperature profile at pressures less than 1 bar is taken from the Voyager radio occultation experiment (Lindal, 1992), with an extrapolation to higher pressures along a pseudo-adiabat. The lapse rate is appropriately adjusted for condensable species. The He to H₂ ratio is 0.157 and the CH₄ molar mixing ratio is 1.8×10^{-3} relative to total abundance (consistent with Atreya et al., 1999, but note that they quote abundances relative to H₂). The mixing ratios for NH₃ and H₂O are adjustable; three times solar abundances are defined to be 5.79×10^{-4} and 4.41×10^{-3} , respectively (Anders and Grevesse, 1989). No loss of NH₃

into the water or a possible NH₄SH cloud is considered. The absorption coefficient and lineshape profile for ammonia is from Spilker, 1993. For water vapor we use an expression based on laboratory data over a range of pressure and temperature applicable to Jupiter down to approximately the 30-bar pressure (500 K temperature) level (Ho et al., 1966; Goodman, 1969). The base of the model atmosphere is arbitrarily placed at 1000 bar, with isothermal conditions assumed below this.

Figure 2 shows nadir-viewing weighting functions for a nominal atmosphere (3 × solar H₂O and NH₃, and no absorption by clouds) and a representative set of frequencies along with their relationship to clouds and Jupiter's pressure–temperature structure. Figure 3a shows the nadir brightness temperature spectrum for this atmospheric model assuming different values for subcloud water and ammonia abundances. As illustrated, a nominal 2% measurement calibration uncertainty that is random with frequency would not enable us to distinguish the differences among the water abundances shown. This conclusion, discussed further below, is consistent with the analysis by de Pater et al.

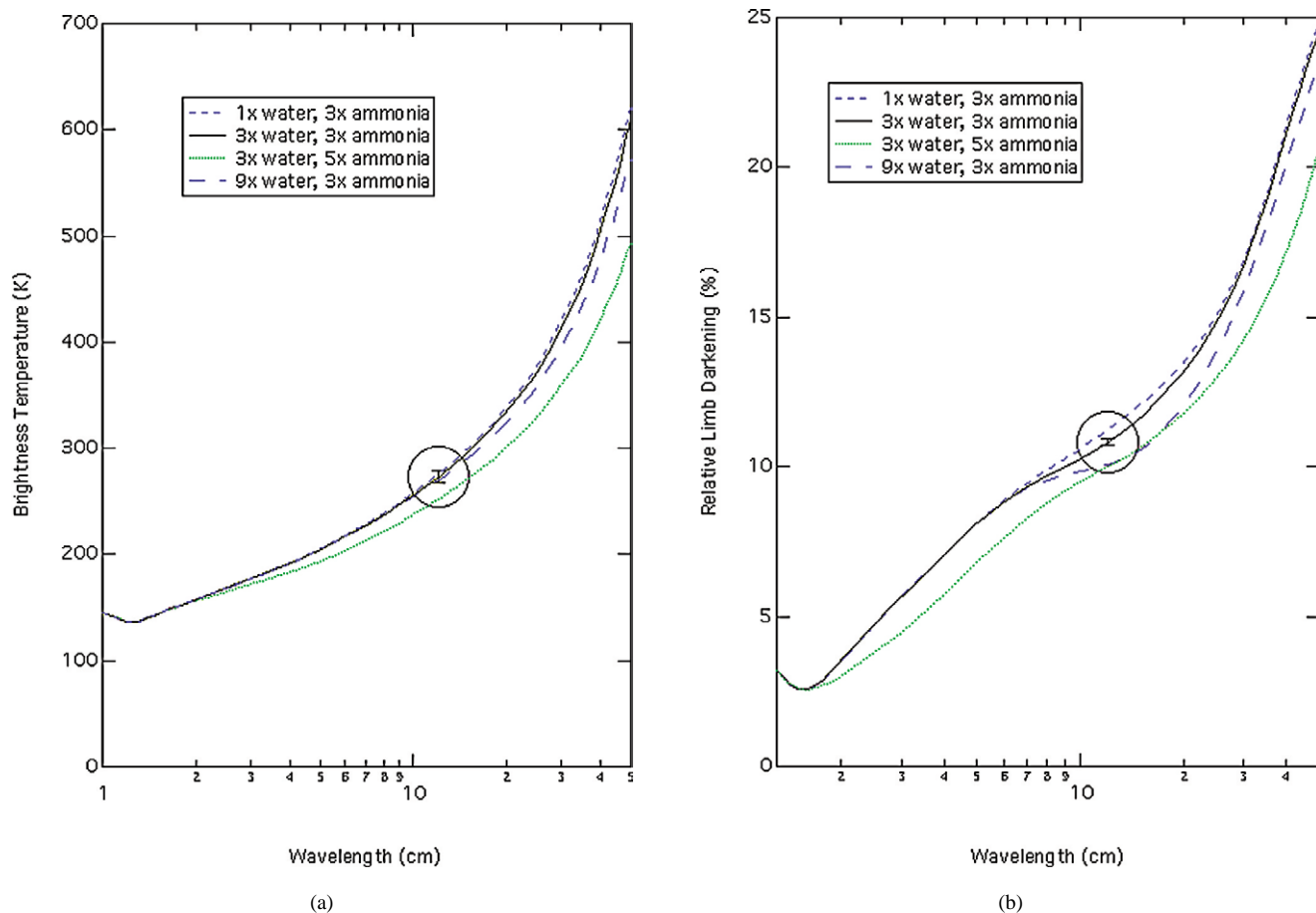


Fig. 3. (a) Nadir brightness temperature spectra for water and ammonia abundance variations on our baseline model (3 × solar ammonia and water). An expected error of 2% (circled) is indicated. The black curve shows the spectrum of the baseline model. The two blue curves show the spectra resulting when the water abundance is changed from the baseline to 1 × (upper curve, short dash) and 9 × (lower curve, long dash) solar, respectively. The green curve (dotted) shows the spectrum when the ammonia abundance in the baseline is increased from 3 × to 5 × solar. (b) Relative brightness R , which is the difference between the brightness at nadir and that at an emission angle of 60°, expressed as a percentage of the nadir brightness, for the same models. An error of 0.1% (circled) is indicated.

(2004), for the interpretation of the disk temperature spectrum.

Figure 3b shows calculations of limb darkening for the same models. The error bar shows the 0.1% relative uncertainty. For convenience in the following discussion we parameterize limb darkening as the difference between the brightness temperature at nadir and that at an emission angle 60° from nadir, normalized by the nadir brightness temperature and expressed as a percentage of the nadir brightness $\{R(\%) = ((T_{b\text{nadir}} - T_{b60^\circ}) / T_{b\text{nadir}}) \times 100\}$ (note that we use the term “limb darkening” throughout to refer to the changing brightness at a single location as the emission angle varies). A measurement precision on the order of 0.1% now enables us to easily distinguish among the model curves.

The limb darkening parameter R is particularly sensitive to the altitude profile of the absorption, and being a differential measurement can be measured with high precision. The distinctive brightness signature in R seen in Fig. 3b for water arises because its scale height is much less within the cloud, where it follows a saturation curve, than in the uniformly mixed region below the cloud. This creates an absorption “ledge” that is seen at wavelengths in the range 10–20 cm where the emission comes mainly from the cloud region. This reduces the limb darkening in this wavelength range because the weighting function is compressed there. For example, in the extreme case of an abrupt increase in absorption with depth the brightness would tend toward that of a uniform disk. In Fig. 3b the dip in limb darkening for the $3 \times$ solar water case relative to that for $1 \times$ solar starts around 5-cm wavelength, peaks at 15 cm, and disappears beyond roughly 30 cm. Figure 2 shows that the weighting function just begins to descend into the water saturation region at around 5 cm, brackets the absorption transition region at 15 cm, and is well into the water constant mixing region by 30 cm. The feature in the $9 \times$ solar case differs from the $3 \times$ solar case in that it peaks at a longer wavelength and extends to longer wavelengths because the model cloud base is at a correspondingly lower and warmer level.

The variation of ammonia abundance is seen to produce a significantly different limb darkening frequency dependence. The weighting function is entirely in the saturation region at wavelengths in the ammonia inversion band centered around 1.3 cm, so that the limb darkening is a minimum at that wavelength. As ammonia abundance is increased the saturation region extends deeper in the atmosphere, decreasing the limb darkening at slightly longer wavelengths. The continued decrease in limb darkening at wavelengths beyond a few centimeters has a different cause, however, which we find to be the different behavior of ammonia and water absorption with pressure and temperature. Specifically, the temperature dependences of our absorption models are proportional to T^{-3} and T^{-5} for ammonia and water respectively. Since ammonia absorption consequently increases more rapidly with depth than water for constant mixing ratio, the ammonia weighting function is more compressed and the limb darkening is reduced.

4. A simple retrieval study

Using a model in which the subcloud water and ammonia abundances are the only free parameters, we performed a simple study to determine the sensitivity of a combined absolute and relative sounding approach. We assumed that the sounding instrument comprises 6 radiometers operating at the same wavelengths for which weighting functions are depicted in Fig. 2. No absorption from cloud particles was assumed. While in a real case we would use the full range of emission angle measurements with appropriate weighting to solve for the abundances, here for simplicity we only considered the measurements at nadir and at 60° emission angle. We assumed a random 2% absolute uncertainty in the nadir brightness measurement at each frequency relative to a model value and a 0.1% relative uncertainty between the nadir brightness and that at 60° . We confirmed the capability to independently retrieve water and ammonia that is apparent in Fig. 3 by using a chi-squared minimization approach to solve for the abundances. We found one-sigma uncertainties in the water and ammonia abundances to be 0.6 and 0.06, respectively, *in units of the solar abundance ratios*. These uncertainties did not vary significantly over the $1 \times$ to $9 \times$ solar water abundance range. They increased by an order of magnitude if only the nadir observations are used, however, confirming our qualitative observation above.

We examined some basic variations on this model to assess its robustness. We find that the water retrieval uncertainty increases by only about a factor of two if we reduce our off-nadir emission angle from 60° to 40° . Figure 3 suggests that the retrieval of water abundance is dominated by the wavelength range shortward of 30 cm. The uncertainty is approximately doubled if we drop our lowest frequency. Large ammonia abundances do not seriously complicate the water abundance retrieval—raising the ammonia abundance from $3 \times$ to $9 \times$ solar only increased the water abundance retrieval errors by a factor of about 1.5. Cloud region properties can be highly variable. Although the relative humidity in the cloud region has an effect on the absolute brightness, the limb darkening is almost unaffected. We found that a cloud relative humidity change from 100% to 20% had a negligible ($< 0.1\%$) effect.

However, the limb darkening is highly sensitive to absorption by cloud liquid if it is present in quantity, as illustrated by the blue curve in Fig. 4. Here we have considered an extreme case based on an uplifted parcel through the cloud region that retains all of its condensed liquid water (Weidenschilling and Lewis, 1973). The estimated absorption for this model results in an absorption spike around the cloud base with a total optical depth of about 0.4 at a wavelength of about 15 cm, for example. The wavelength-dependent effect on relative brightness seen in the figure is sharpened, reducing its half-width in wavelength relative to the difference between $3 \times$ and $9 \times$ solar water in Fig. 3, and shifting it to shorter wavelengths as well. Such a difference in the frequency-dependent signature is expected because

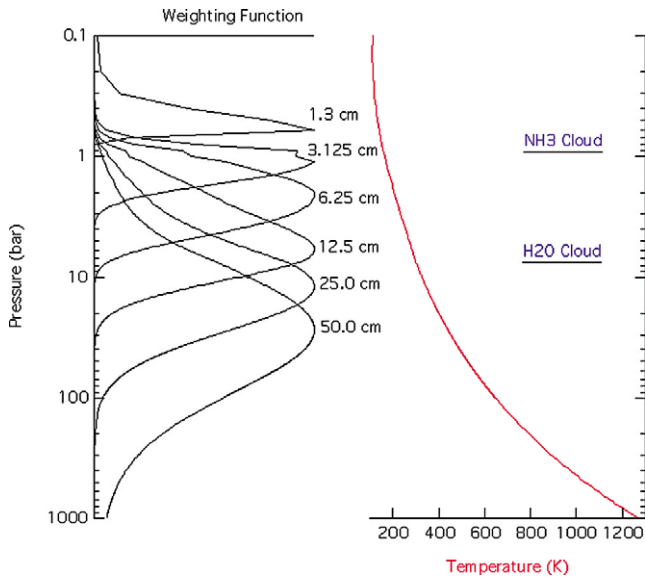


Fig. 2. Nadir-viewing weighting functions for wavelengths in the range 1 to 50 cm (labeled curves on the left), along with temperature and cloud locations, calculated for our baseline model atmosphere with $3 \times$ solar abundances of water and ammonia. The weighting functions are the vertical derivatives of the atmospheric transmittance normalized to a peak value of unity.

the liquid absorption is present in a narrower and higher altitude region.

5. Discussion

Jupiter's atmosphere is more complex than the baseline model considered above. Ammonia is likely far from saturation on the average in the cloud region (Achterberg et al., 2003; Hofstadter et al., 2003; Gibson et al., 2004). Water can be expected to behave similarly; in fact, an interpretation of the low Galileo probe result for water concentration at about 20 bars (Niemann et al., 1998) is that its concentration was greatly reduced from its global abundance even at a point well below the nominal water cloud base by dynamical effects (Atreya et al., 1997; Showman and Ingersoll, 1998; Showman and Dowling, 2000). Unforeseen absorbing cloud constituents may be present (e.g., in the ammonium hydro-sulfide cloud region, or due to other constituents at levels below the water clouds). Atmospheric dynamics will drive departures in the lapse rate in potentially significant ways. These are complications that must be dealt with in the retrieval of atmospheric parameters from microwave sounding, and very little is known about them (de Pater et al., 2004).

In essence microwave sounding enables us to determine only the opacity profile coupled with temperature, and it is the interpretation of this profile in the context of a constrained atmospheric model that enables the retrieval of atmospheric parameters. de Pater et al. (2004) have discussed the difficulty of this using whole-disk averages (as would be done using ground-based observations). However, along

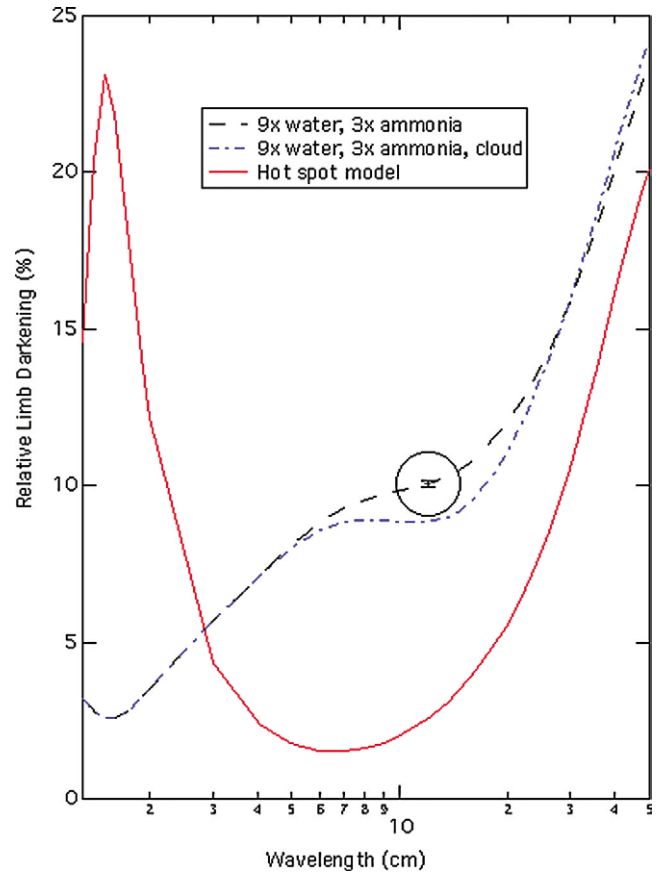


Fig. 4. Relative brightness R for other possible variations on our baseline model. The black (long dash) curve shows the spectrum of a model with $3 \times$ solar ammonia and $9 \times$ water. The blue curve (dot-dash) is the same model except that it includes absorption by liquid water in the cloud region as discussed in the text. The red curve shows the very different spectrum for a “hot spot” region with the water and ammonia distributions similar to those measured by the Galileo probe.

with the much higher sensitivity to atmospheric properties demonstrated above, microwave sounding from an orbiting platform has the advantage that the unknown and spatially variable properties of the atmosphere outlined above can be addressed by observing all states of the atmosphere and not just a global average. We envision an experiment in which a significant fraction of the atmospheric opacity is profiled with temperature with the resolution indicated in Fig. 1. This would provide an exploration, on a global scale, of these features of the deep atmosphere at the same time as we refine our models for the interpretation of key parameters such as the global water abundance. Investigation of these features directly addresses outstanding questions fundamental to understanding the dynamics and deep circulations of the planet (e.g., Allison, 2000; Ingersoll et al., 2000). The determination of water abundance with sufficient accuracy to distinguish between a nominal abundance of $3 \times$ solar, and the cases of $1 \times$ solar or less, and $9 \times$ solar or more, is needed to discriminate among models for Jupiter's origin (Owen et al., 1999; Gautier et al., 2001; Owen and Encrenaz, 2003; Hersant et al., 2004). Hence, while we have demonstrated

that we can achieve very high precision in a constrained model, much less precision is needed to obtain a scientifically important result.

The identification of water in our simple model depended on the uniform mixing of water up to its saturation level, a condition that may be typical of upwelling regions. The interpretation of subcloud vapor abundance can be complicated by the presence of liquid water, but as illustrated in Fig. 4 these two sources of opacity can be distinguished by their different frequency dependences for the limb darkening. Microwave opacity from a cloud at a different temperature such as a putative ammonium hydrosulfide cloud can be identified because its limb-darkening signature will appear in a different wavelength range. By extension, although the magnitude of cloud absorption is difficult to model and predict, we expect to be able to use the combined relative and absolute measurements to locate the altitude of any cloud-like absorption spike to both facilitate its identification and remove its effect from the water abundance determination. Variations with latitude in conjunction with vertical structure models can be particularly useful in the identification of clouds.

Downwelling can lead to the drying out of both ammonia and water, with an extreme example given by the Galileo probe hot spot. The depths to which water is depleted in dry regions can be investigated; for example, the present approach would allow one to determine whether or not the Galileo results are valid on a global scale. The limb darkening parameter computed for such a case (red curve in Fig. 4) gives a much different emission angle dependence from the nominal models. In the worst case, the local meteorology could conspire to produce the same mixing ratio profile for both species at a point or two on the planet. Even then the different pressure-temperature dependences of the absorption in the present model could in principle lead to the separation of these two as discussed in Section 3, although the temperature dependence of ammonia opacity is presently theoretical and not founded on laboratory data. Better knowledge of the lineshapes of water and ammonia will greatly facilitate the interpretation of the data.

6. Conclusions

Passive microwave sounding from a spacecraft is a promising new technique for determining the deep water abundance in Jupiter to at least an accuracy that enables us to discriminate among models for Jupiter's origin. Because the observations can probe the horizontal structure of temperature and composition, microwave sounding from a spacecraft provides a possible approach to the investigation of outstanding questions fundamental to understanding the dynamics and deep circulations of the planet as well. There are requirements on a spacecraft microwave instrument for stability and antenna design, but these appear straightforward

through the frequency range of interest, noting that at longer wavelengths (beyond roughly 30 cm, or 1 GHz) increasing synchrotron emission and the need for larger aperture areas become important. Better knowledge of the microwave opacity of water and ammonia under conditions in the jovian atmosphere are needed to fully exploit this approach, and new laboratory measurements of both the pressure and temperature dependences of these constituents are recommended.

Acknowledgments

The authors thank S. Atreya, J. Lunine, T. Spilker, and T. Owen for their advice and thoughtful comments on this work. We also thank R. Young, I. de Pater, M. Marley, R. Freedman, and D. DeBoer for allowing us to test our opacity calculations against theirs, and for several useful discussions. Finally we thank I. de Pater and an anonymous referee for their helpful comments and aid in the improvement of this paper. This work was carried out at the Jet Propulsion Laboratory, California Institute of Technology, under a contract with the National Aeronautics and Space Administration.

References

- Achterberg, R.K., Conrath, B.J., Gierasch, P.J., Flasar, F.M., 2003. Cassini CIRS observations of ammonia in Jupiter's upper troposphere. *Bull. Am. Astron. Soc.* 35, 997.
- Allison, M., 2000. A similarity model for the windy jovian thermocline. *Planet. Space Sci.* 48, 753–774.
- Anders, E., Grevesse, N., 1989. Abundances of the elements-meteoritic and solar. *Geochim. Cosmochim. Acta* 53, 197–214.
- Atreya, S., Wong, M.H., Owen, T., Niemann, H., Mahaffy, P., 1997. Chemistry and clouds of the atmosphere of Jupiter: a Galileo perspective. In: Barbieri, C., Rahe, J.H., Johnson, T.V., Sohus, A.M. (Eds.), *The Three Galileos: The Man, The Spacecraft, The Telescope*. Kluwer Academic, Norwell, MA, pp. 249–260.
- Atreya, S.K., Wong, M.H., Owen, T.C., Mahaffy, P.R., Niemann, H.B., de Pater, I., Drossart, P., Encrenaz, Th., 1999. A comparison of the atmospheres of Jupiter and Saturn: deep atmospheric composition, cloud structure, vertical mixing, and origin. *Planet. Space Sci.* 47, 1243–1262.
- Berge, G.L., Gulkis, S., 1976. Earth-based radio observations of Jupiter: millimeter to meter wavelengths. In: Gehrels, T. (Ed.), *Jupiter*. Univ. of Arizona Press, Tucson, pp. 621–692.
- de Pater, I., Dunn, D., Zahnle, K., Romani, P., 2001. Comparison of Galileo probe data with ground-based radio measurements. *Icarus* 149, 66–78.
- de Pater, I., DeBoer, D., Marley, M., Freedman, R., Young, R., 2004. Retrieval of water in Jupiter's deep atmosphere using microwave spectra of its brightness temperature. *Icarus*. This issue.
- Gautier, D., Hersant, F., Mousis, O., Lunine, J.I., 2001. Enrichments in volatiles in Jupiter: a new interpretation of the Galileo measurements. *Astrophys. J.* 550, L227–L230. Erratum: *Astrophys. J.* 559 (2001) L183.
- Gibson, J., Welch, W.J., de Pater, I., 2004. Accurate jovian flux measurements at 11 cm show ammonia to be sub-saturated in the upper atmosphere. *Icarus*. Submitted for publication.
- Goodman, G.C., 1969. Models of Jupiter's atmosphere. PhD thesis. University of Illinois.

- Hersant, F., Gautier, D., Lunine, J.I., 2004. Enrichment in volatiles in the giant planets of the Solar System. *Planet. Space Sci.* 52, 623–641.
- Ho, W., Kaufman, I.A., Thaddeus, P., 1966. Laboratory measurement of microwave absorption in models of the atmosphere of Venus. *J. Geophys. Res.* 71, 5091–5108.
- Hofstadter, M.D. 1992. Microwave observations of Uranus. PhD thesis. California Institute of Technology.
- Hofstadter, M.D., Butler, B.J., 2003. Seasonal change in the deep atmosphere of Uranus. *Icarus* 165, 168–180.
- Hofstadter, M.D., Readhead, T., Gulkis, S., Reeves, R., 2003. Humidity above the jovian NH₃ clouds from radio measurements near 1 cm. *Bull. Am. Astron. Soc.* 35, 1014.
- Ingersoll, A.P., Gierasch, P.J., Banfield, D., Vasavada, A.R., the Galileo Imaging Team, 2000. Moist convection as an energy source for the large-scale motions in Jupiter's atmosphere. *Nature* 403, 630–632.
- Janssen, M.A., Ruf, C.S., Keihm, S.J., 1995. TOPEX/Poseidon microwave radiometer. II. Antenna pattern correction and brightness temperature algorithm. *IEEE Trans. Geosci. Remote Sensing* 33, 138–146.
- Janssen, M.A., Bolton, S.J., 19 colleagues, 2001. Cassini RADAR/radiometer and VLA observations of Jupiter's synchrotron emission. In: Rucker, H.O., Kaiser, M.L., LeBlanc, Y. (Eds.), *Planetary Radio Emissions V*. Verlag der Osterreichischen Akademie der Wissenschaft, Vienna, pp. 229–236.
- Keihm, S.J., Zlotnicki, V., Ruf, C.S., 2000. TOPEX microwave radiometer performance evaluation, 1992–1998. *IEEE Trans. Geosci. Remote Sensing* 38, 1379–1386.
- Levin, S.M., Bolton, S.J., Bhattacharya, B., Gulkis, S., Klein, M.J., Thorne, R.M., 2001. Modeling Jupiter's synchrotron emission. *Geophys. Res. Lett.* 28 (5), 903–906.
- Lindal, G.F., 1992. The atmosphere of Neptune: an analysis of radio occultation data acquired with Voyager 2. *Astron. J.* 103, 967–982.
- Niemann, H.B., Atreya, S.K., Carignan, G.R., Donahue, T.M., Haberman, J.A., Harpold, D.N., Hartle, R.E., Hunten, D.M., Kasprzak, W.T., Mahaffy, P.R., Owen, T.C., Way, S.H., 1998. The composition of the jovian atmosphere as determined by the Galileo mass spectrometer. *J. Geophys. Res.* 103 (E10), 22831–22845.
- Owen, T.C., Encrenaz, T., 2003. Element abundances and isotope ratios in the giant planets. *Space Sci. Rev.* 106, 121–138.
- Owen, T.C., Mahaffy, P., Niemann, H.B., Atreya, S.K., Donahue, T.M., BarNun, A., de Pater, I., 1999. A new constraint on the formation of giant planets. *Nature* 402, 269–270.
- Ruf, C.S., Keihm, S.J., Janssen, M.A., 1995. TOPEX/Poseidon microwave radiometer (TMR): I. Instrument description and antenna temperature calibration. *IEEE Trans. Geosci. Remote Sensing* 33, 125–137.
- Showman, A.P., Dowling, T.E., 2000. Nonlinear simulations of Jupiter's 5- μ m hot spots. *Science* 289, 1737–1740.
- Showman, A.P., Ingersoll, A.P., 1998. Interpretation of Galileo probe data and implications for Jupiter's dry downdrafts. *Icarus* 132, 205–220.
- Spilker, T.R., 1993. New laboratory measurements on ammonia's inversion spectrum, with implications for planetary atmospheres. *J. Geophys. Res.* 98, 5539–5548.
- Tanner, A.B., 1998. Development of a high-stability water vapor radiometer. *Radio Sci.* 33 (2), 449–462.
- Tanner, A.B., Riley, A.L., 2003. Design and performance of a high-stability water vapor radiometer. *Radio Sci.* 38 (3), 1–12.
- Weidenschilling, S.J., Lewis, J.S., 1973. Atmospheric and cloud structures of the jovian planets. *Icarus* 20, 465–476.